



Metronidazole and Cephalexin degradation by using of Urea/TiO₂/ZnFe₂O₄/Clinoptilolite catalyst under visible-light irradiation and ozone injection

Maryam Aram^a, Mehrdad Farhadian^{a,*}, Ali Reza Solaimany Nazar^a, Shaharam Tangestaninejad^b, Parisa Eskandari^a, Byong-Hun Jeon^c

^a Department of Chemical Engineering, Faculty of Engineering, University of Isfahan, Isfahan, Iran

^b Department of Chemistry, Catalysis Division, University of Isfahan, Iran

^c Department of Earth Resources and Environmental Engineering, Hanyang University, Seoul, South Korea

ARTICLE INFO

Article history:

Received 26 November 2019

Received in revised form 5 February 2020

Accepted 21 February 2020

Available online 22 February 2020

Keywords:

Metronidazole

Cephalexin

ZnFe₂O₄

Photocatalyst

Ozonation

Urea/TiO₂

ABSTRACT

Cephalexin (CEX) and metronidazole (MNZ) degradation were photodegraded using the synthesized Urea/TiO₂/ZnFe₂O₄/Clinoptilolite catalyst under visible light irradiation. Diffuse reflectance ultraviolet–visible spectroscopy (UV–Vis DRS) and photoluminescence (PL) analysis approved the modification of TiO₂ by Urea and ZnFe₂O₄ compounds increased the absorption edge of catalyst to 590 nm and decreased the electron–hole recombination rate. The results showed the degradation efficiencies of ozonation process for the metronidazole and cephalexin removal were obtained 36% and 39%, respectively. The photocatalyst activity of Urea/TiO₂/ZnFe₂O₄/Clinoptilolite (Zeolite) under visible light irradiation was determined 70% for metronidazole and 74% for cephalexin degradation. Furthermore, the combination of ozonation process and photocatalyst degradation under visible light irradiation showed high potential for the antibiotics degradation (94% for metronidazole and 95% for cephalexin) due to the increase in the generation of reactive species and synergistic effect between photocatalysis and ozonation processes. The response surface methodology (RSM) results revealed the removal efficiency of both pollutants were highly dependent on pH, irradiation time, catalyst concentration and initial antibiotics concentration. First order kinetics model described the degradation process and the rate constants were 0.0196 and 0.0243 min⁻¹ for the metronidazole and cephalexin removal, respectively.

© 2020 Elsevier B.V. All rights reserved.

1. Introduction

The presence of contaminants, especially pharmaceutical compounds in water streams is rapidly increasing due to their wide application in human and veterinary medicine [1–3]. Personal hygiene products, pharmaceutical industry waste, hospital waste and therapeutic drugs lead to the contamination of water and wastewaters by pharmaceutical compounds [4]. Therefore, it is more likely that most urban wastewaters are polluted with pharmaceutical compounds, especially antibiotics. It is estimated about 100,000–200,000 tons of antibiotics have been consumed worldwide over the last 50 years and only <30% of them are metabolized in the body and a large percentage of them are active after excretion [5,6]. Among antibiotics, MNZ and CEX with a wide spectrum of antibacterial activity and high water solubility are the most commonly-used products for treating infectious diseases (2670 tons of CEX was consumed in China in 2013, 163 tons of CEX

was consumed in Brazil in 2005) [2,7–11,62]. The presence of these antibiotics and their continues input in aquatic environment could result in the ever-increasing of their accumulation in the environment leading to a potential risk for ecosystem, human and animal in both low and high concentration because these compounds are considered as chronic toxic, carcinogenic, mutagenic and fatal abnormalities elements [1,11–17]. As a result, treatment of the wastewaters polluted by antibiotics is a vital issue. However, the conventional wastewater treatment methods have shown poor performance to degrade these materials due to the production of secondary pollutants, the bacterial resistance property and poor biodegradability nature of metronidazole and cephalexin [1,18,19]. Consequently, highly efficient alternative methods should be employed to degrade pharmaceutical compounds from wastewaters. Advanced oxidation processes (AOPs) have a high potential to degrade environmentally persistent contaminants and convert them to harmless compounds by using produced powerful oxidizing agents especially hydroxyl radicals which react with various contaminants with the rate constants in the order of 10⁶–10⁹ M⁻¹ s⁻¹ [1,8,20,21]. There are various types of AOPs classified as two groups of

* Corresponding author.

E-mail address: m.farhadian@eng.ui.ac.ir (M. Farhadian).

homogenous and heterogeneous phases that are widely applied for water and wastewater treatments such as photolysis process (UV), ozone-based AOPs (O_3/UV , O_3/H_2O_2 , and $O_3/H_2O_2/UV$), hydrogen peroxide-based purification method (H_2O_2/UV), photocatalysis under ultraviolet, visible light or solar irradiation (TiO_2/UV and $TiO_2/H_2O_2/UV$ systems) and so on [23]. The ways in which reactive species are generated, the concentration of produced oxidizing compounds and their degradation efficiency of these various types of AOPs are different [23]. Photolysis by itself has shown low mineralization performance and much smaller degradation rate compared to simple ozonation for water and wastewater treatment [24]. Besides, the oxidation-reduction potential of $\bullet OH$ radicals, O_3 and H_2O_2 are 2.85 eV, 2.07 eV and 1.77 eV respectively confirming the lower reactivity of hydrogen peroxide than that of two oxidizers for decomposition of pollutants in wastewaters [25]. Therefore, it seems that simple O_3 process is more effective method for water purification in comparison with H_2O_2 or UV light process. Ozone has the high oxidizing power and selectivity toward various contaminants and can degrade pollutants by direct ozonation and indirect use of hydroxyl radicals [23,25]. However, due to the low solubility of ozone in water, low water resistance and the slow reaction between ozone and some compounds, the single ozonation process is not recommended as a main water purification approach and it is better to combine ozone injection method with other AOPs, especially photocatalysis [15,23]. The heterogeneous photocatalysis processes which are based on the generation of e^-/h^+ pairs under light irradiation, transformation of photo-excited charges to the surface of catalyst, the redox reaction of the charges and the formation of reactive compounds to decompose pollutants can be combined by ozone process to improve oxidizing ability and obtain higher mineralization and degradation rate [26]. TiO_2 is considered as a promising catalyst for photocatalytic degradation owing to its excellent chemical and thermal stability and strong oxidation capacity [27]. Although TiO_2 is among the most widely-used materials for photodegradation process, its performance for the visible application is greatly restricted due to its wide band gap which brings some drawbacks [28–32]. The surface photoactivation fails to generate electron-hole pairs. The low quantum yield rate of the visible light activation is another major drawback. A low photocatalytic activity due to the weak separation efficiency of photocarriers and high recombination rate of electron hole pairs could limit the practical application of TiO_2 because when the recombination of electron and hole pairs occurs the energy will release as heat and decomposition will be not carried out [33–35]. Consequently, there is the necessity to modify the wide band gap of TiO_2 and minimize e^-/h^+ recombination rate by doping TiO_2 with nonmetal elements such as nitrogen or semiconductor like zinc ferrite ($ZnFe_2O_4$) that can have a positive effect on decreasing the band gap energy, extending the absorption edge to the visible light edge and improvement of photoreaction rate [36–38]. The electronic structure of $ZnFe_2O_4$ and its narrow band gap, its visible-light response and good photochemical stability make it an appropriate option for doping with TiO_2 [36,39,40]. Besides, spinel crystal structure of $ZnFe_2O_4$ plays a vital role in enhancing the photocatalytic activity owing to the available extra catalytic sites by virtue of the crystal lattice [39]. Moreover, nitrogen doped TiO_2 is also considered as high efficient visible-driven photocatalyst due to the similar ionic size of nitrogen with oxygen and lower ionization energy than O_2 which not only can effectively control on chemical and electronic state and surface structure of TiO_2 but also the similar ionic size can have a key role in the reduction of the generation of electron and hole recombination centers [41,42].

Nanostructured photocatalysts offer many advantages than the photocatalysts with average size more than nano such as high surface/volume ratio, excellent optical behaviors, higher activity and degradation rate [14,35]. Nonetheless, due to the aggregation tendency of N- $TiO_2/ZnFe_2O_4$ nanostructure, the catalyst should be supported on materials to prevent the aggregation of the catalyst, facilitate its recovery

process and make it as a commercial compound [43]. Clinoptilolite as a type of natural zeolite could be considered as a supporting material due to its structure and high stability [2,28].

In recent years, the combination of various types of AOPs has been applied to enhance the performance of this method for wastewater treatment [43,44]. The combination of photocatalytic oxidation and ozone processes known as the most advanced oxidation processes could have significant effects on accelerating the photoreaction rate and improving the degradation efficiency by using a compound as a catalyst and ozone as both an oxidizing agent and radical producer to generate more reactive species [15,45–47]. The catalytic ozonation with the great synergism between the photocatalysis and ozonation process not only degrades the pollutants and intermediate compounds effectively and is a great method to address the problems of single ozonation process, but also it is less affected by the scavenging phenomenon or self-radicalization [15]. There are some studies with regard to applying different types of AOPs to treat pharmaceutical compounds from polluted water [48,49]. However, there has been no study on evaluation the performance of N- $TiO_2/ZnFe_2O_4$ /zeolite photocatalyst under visible light and its combination with ozonation process for comparison the performance of this process for metronidazole and cephalexin degradation. Moreover, previous studies have adopted the traditional one-factor-at-a-time approach to obtain the optimization conditions of process which not only makes the experiments too time-consuming and expensive due to reagent costs but also it does not determine the interactions between the operational factors and thereby disabling the assessment of interactive effects of factors [28,50,51]. Response surface methodology (RSM), based on statistical designs of experiments (DOEs), which designs experiments and assesses the responses, model process and optimization conditions is an efficient technique that could be replaced with an inefficient one-factor-at-a-time method [50,53].

The aim of this paper is the synthesis of visible-light absorbing N- $TiO_2/ZnFe_2O_4$ nanostructure supported on zeolite to evaluate the photocatalytic ozonation for both metronidazole and cephalexin degradation. The RSM design was adopted to optimize four operational factors including initial antibiotics concentration, pH, irradiation time and N- $TiO_2/ZnFe_2O_4$ /zeolite concentration at which the degradation efficiencies of metronidazole and cephalexin were considered as responses. The kinetic study and photodegradation mechanism for both pollutants were investigated. The photocatalytic activity of bare TiO_2 , N- TiO_2 , bare $ZnFe_2O_4$, N- $TiO_2/ZnFe_2O_4$ and N- $TiO_2/ZnFe_2O_4$ /zeolite was determined to study the effect of modification and stabilization of TiO_2 with nitrogen, zinc ferrite and zeolite. The reusability of N- $TiO_2/ZnFe_2O_4$ /zeolite catalyst, the effects of the weight ratios of N: TiO_2 and N- TiO_2 : $ZnFe_2O_4$ were also evaluated. The effectiveness of different types of AOPs including UV-Vis light, O_3 , N- $TiO_2/ZnFe_2O_4$ /zeolite/UV-Vis, O_3 /UV-Vis and N- $TiO_2/ZnFe_2O_4$ /zeolite/ O_3 /UV-Vis on the removal of MNZ and CEX were compared.

2. Experimental

2.1. Preparation of N- $TiO_2/ZnFe_2O_4$ /zeolite composite photocatalysts

$ZnFe_2O_4$ nanoparticles were synthesized by the following procedures. $Fe(NO_3)_3 \cdot 9H_2O$ (Merck, purity 99%, 1 M, 24.8 mL) and $Zn(NO_3)_2 \cdot 4H_2O$ (Merck, purity 99%, 1 M, 12.4 mL) were mixed and 55.8 mL citric acid (Merck, purity 99%, 1 M) with molar ratio 1:2 of Fe/Zn: citric acid was added to the solution and continuously stirred at 100 °C for 1 h. The solution was dried inside an electric oven at 120 °C for 24 h. The sample was calcined at 500 °C for 2 h inside a muffle furnace and the $ZnFe_2O_4$ nanoparticle was obtained.

N- $TiO_2/ZnFe_2O_4$ nanocomposites were prepared by the sol-gel method. The procedure of N- $TiO_2/ZnFe_2O_4$ synthesis for weight ratios of 1:3 for N: TiO_2 and 2:1 for N- TiO_2 : $ZnFe_2O_4$ is as follows: TBOT (Merck, purity 99%, 12.86 mL), $ZnFe_2O_4$ (2 g) and urea (Merck, purity 99%, 2.3 g), as a nitrogen source, were separately added to 16, 9 and

4 mL ethanol (Merck, purity 99%) respectively. After 1 h sonication of these solutions at 25 °C, the mixture of deionized water (3 mL) and HCl (Merck, 12 M, 1 mL) was added to the urea solution. This solution and ZnFe₂O₄ solution were added dropwise into the TBOT solution. The solution was mixed using stirrer-heater at 80 °C for 3 h. The content was cooled to room temperature, filtered and washed with deionized water for several times followed by drying inside an electric oven at 80 °C for 18 h and calcination of N-TiO₂/ZnFe₂O₄ at 450 °C for 2 h inside a muffle furnace.

The stabilization of N-TiO₂/ZnFe₂O₄ nanostructure on zeolite was carried out by adding 1 g N-TiO₂/ZnFe₂O₄ and 9 g zeolite into ethanol followed by sonication of the mixture for 1 h at room temperature. The content was dried by rotary evaporator and N-TiO₂/ZnFe₂O₄/zeolite nanoparticles were obtained.

2.2. Characterization

The X-ray diffraction (XRD) patterns of as-prepared samples were conducted (BrukerD-8 Advance, Germany) in the 2θ range of 10–80° at room temperature to determine their phase crystallinity and phase structure. The X-ray Fluorescence (XRF) (Bruker S4-Pioneer, Germany) analysis detected the chemical composition and structure of the chemical compounds. The morphology of samples was examined by using field-emission scanning electron microscope (FESEM) (Philips XL 30 and S-4160) equipped with Energy Dispersive X-ray applied to determine the composition of samples. The Fourier transform infrared (FTIR), (Jasco, 6300, Japan) was applied in the 400–4000 cm⁻¹ region to identify the surface functional groups and the surface chemical characteristics of the nanocomposite. The light absorption of the catalysts was estimated from diffuse reflectance ultraviolet–visible spectroscopy (UV–vis DRS) (V-670, Jasco, Japan). Photoluminescence emission spectra (PL) were measured at room temperature using a fluorescence spectrometer (Perkin Elmer LS55) to assess the recombination rate situation of catalysts at an excitation wavelength of 410 nm.

2.3. Photocatalytic degradation experiment

The photocatalytic reactions were carried out in a cylindrical quartz vessel surrounded with a water circulation system and equipped with a digital thermometer at the top of the reactor to maintain the reaction temperature constant at 25 °C. The reactor contained pollutants solution (metronidazole or cephalexin) (Table 1) with desired concentrations and pH. The N-TiO₂/ZnFe₂O₄/zeolite nanoparticles were suspended to the solution using a magnetic heater-stirrer. The setup included an ozone system (ARDA company), consisted of an ozone generator, an ozone analyzer to determine inlet and outlet gaseous ozone concentrations, a gas-washing trap, and a gas-flow controller. Ozone was generated from pure oxygen (99.9%) by using an ozone generator and bubbled into the liquid by means of a porous glass disk diffuser with a gas flow of 500 mg/h placed at the upper part of the reactor. Potassium iodide (KI, 2%) was used for reacting with residual ozone. The solution was stirred under dark conditions for 30 min to ensure the accomplishment of an adsorption–desorption equilibrium. Two visible LED lamps

(200 W, light intensity: 400 lm per m²) placed in two sides of the reactor and the lights were illuminated for a specific time through intervals. Fig. 1 shows visible emission spectrum measured by a Jaz UV/Visible spectrophotometer device (Ocean Optics Inc., Japan). The highest emission peak is observed at 532 nm. The schematic of the photoreactor is shown in Fig. 2. After completion of the reaction time, the solution was centrifuged to separate the catalyst using a centrifuge device (HANIL SUPRA 22K) at 8000 rpm for 10 min. The metronidazole and cephalexin concentrations were measured by a spectrophotometer device (V-570, Jasco, Japan) using calibration curve at the maximum wavelength of 320 nm and 273 nm for metronidazole and cephalexin, respectively. The photocatalytic degradation efficiency was calculated according to Eq. (1).

$$\text{Removal (\%)} = \left(1 - \frac{C_t}{C_0}\right) \times 100 \quad (1)$$

where C₀ and C_t are the initial and the final concentrations of metronidazole (or cephalexin) in the solution, respectively.

2.4. Design of experiments

The Box-Behnken design, the most widely-used form of RSM design, was chosen to assess the effect of four independent factors, initial pollutant concentration (metronidazole or cephalexin), nanocatalyst concentration, irradiation time, and pH, at three levels of low (−1), medium (0) and high (+1) and their interactions on the response (pollutant degradation efficiency). Table 2 provides information about the operating ranges and levels of the independent variables of this study. The selected level values for each factor were obtained based on primary experiments. The total number of the experimental runs (N) was obtained using the following equation.

$$N = 2k(k-1) + cp \quad (2)$$

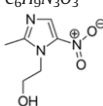
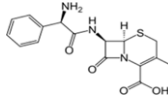
where, k and cp are the number of factors and the replication number of the central point, respectively [28]. In this study, the number of 30 experimental runs was designed according to the Eq. (2). The significance of the independent factors and their interactions on the response as well as the accuracy of the regression model were evaluated using analysis of variance (ANOVA) statistical testing of the model in the form of linear, squared and interaction terms. The optimum conditions of the factors were determined by solving the regression equation and by analyzing the response surface plots as well.

3. Results and discussion

3.1. Characterization of the photocatalyst

The XRD patterns of ZnFe₂O₄, N-TiO₂, N-TiO₂/ZnFe₂O₄, and N-TiO₂/ZnFe₂O₄/zeolite are shown in Fig. 3. The diffraction patterns of ZnFe₂O₄, N-TiO₂/ZnFe₂O₄ and N-TiO₂/ZnFe₂O₄/zeolite confirm the peaks at 2θ = 30.07°, 35.58°, 42.99°, 53.28°, 56.87°, and 62.42° were

Table 1
Characteristics of the pollutants.

| Antibiotic name | Metronidazole | Cephalexin |
|-----------------------------------|---|---|
| Chemical formula | C ₆ H ₉ N ₃ O ₃ | C ₁₆ H ₁₇ N ₃ O ₄ S |
| Structure |  |  |
| Solubility (mg/L) | 7020 | 1790 |
| λ _{max} (absorbance)(nm) | 320 | 273 |
| pK _a | 2.5 | 2.6, 6.9 |
| Molecular weight (g/mol) | 171.15 | 347.39 |

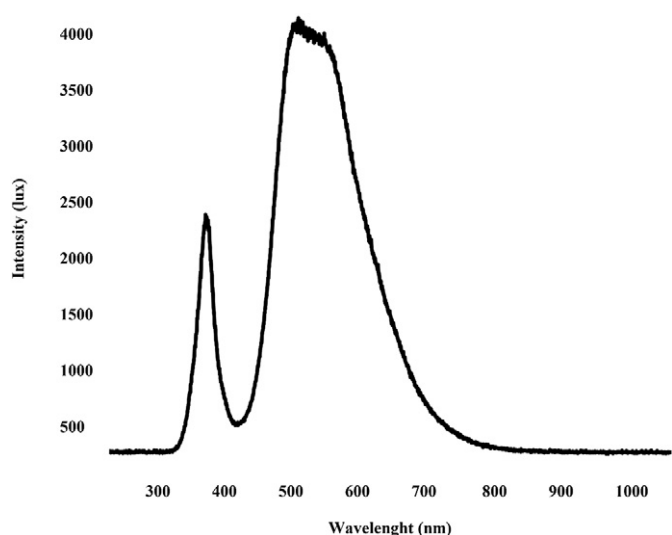


Fig. 1. Emission spectrum of visible light.

Table 2
Experimental ranges and levels of the process factors.

| Factors | Symbol | Levels | | |
|---|--------|--------|-----|-----|
| | | -1 | 0 | 1 |
| Initial antibiotic concentration (mg/L) | A | 10 | 50 | 100 |
| Initial catalyst concentration (g/L) | B | 1 | 1.5 | 2 |
| Time (min) | C | 60 | 90 | 120 |
| pH | D | 4 | 7 | 10 |

zeolite (Fig. 4) revealed the absorbance peaks in the spectral region of 1600–1650 and 3430–3500 cm^{-1} were assigned to the bending and stretching vibrations of O–H [36,42]. The absorbance peak at 545 cm^{-1} corresponded to the Fe–O vibration bond in ZnFe_2O_4 , $\text{N-TiO}_2/\text{ZnFe}_2\text{O}_4$, and $\text{N-TiO}_2/\text{ZnFe}_2\text{O}_4/\text{zeolite}$. The wide absorbance peak in the range of 300–800 cm^{-1} was corresponded to the Ti–O–Ti vibration bond in N-TiO_2 , $\text{N-TiO}_2/\text{ZnFe}_2\text{O}_4$, and $\text{N-TiO}_2/\text{ZnFe}_2\text{O}_4/\text{zeolite}$ whereas no peaks were observed corresponding to the N–H groups of urea molecules adsorbed onto the surfaces of the N-doped material [36,42]. The sharp band at 1444 cm^{-1} implied the presence of nitrate (NO_3^-) group. The peaks at 465, 722, 1068, and 3624 cm^{-1} in $\text{N-TiO}_2/\text{ZnFe}_2\text{O}_4/\text{zeolite}$ were attributed to the internal vibration of (Si, Al)–O bending, Al–O, Si–O–Si, and Si–OH or Al–OH approving the presence of zeolite [2,28,54]. The FESEM images of ZnFe_2O_4 , N-TiO_2 , $\text{N-TiO}_2/\text{ZnFe}_2\text{O}_4$, and $\text{N-TiO}_2/\text{ZnFe}_2\text{O}_4/\text{zeolite}$ (Fig. 5) showed irregular-shaped crystallite with slight agglomeration. The FESEM image of ZnFe_2O_4 revealed uniform particle network with an average particle size of 25–50 nm. The N-TiO_2 had the agglomeration network of spherical shapes and the size of the catalyst was mainly <40 nm. Moreover, the FESEM image of $\text{N-TiO}_2/\text{ZnFe}_2\text{O}_4$ depicted porous nanostructure with variable changes compared to those of ZnFe_2O_4 and N-TiO_2 implying the ZnFe_2O_4 nanoparticles were uniformly doped on the surface of N-TiO_2 . Besides, the comparison of FESEM images of Fig. 5a, b, with those of Fig. 5c confirmed the successful distribution of N-TiO_2 and ZnFe_2O_4 on the surface of zeolite. The results of EDX spectra (Fig. 5d) further verified the presence of N, O, Ti, Fe, Zn (related to semiconductors) and Si, Al (related to zeolite) and also showed the N-TiO_2 and

corresponded to Franklinite phase of ZnFe_2O_4 (JCPDS 77-0011). The diffraction peaks at 25.40°, 38.00°, 48.00°, and 55.19° in the XRD reflections of N-TiO_2 , $\text{N-TiO}_2/\text{ZnFe}_2\text{O}_4$, and $\text{N-TiO}_2/\text{ZnFe}_2\text{O}_4/\text{zeolite}$ were fully matched with anatase phase of TiO_2 (JCPDS 21-1272) and no rutile phase was observed. The XRD patterns of $\text{N-TiO}_2/\text{ZnFe}_2\text{O}_4/\text{zeolite}$ also approved the peaks at $2\theta = 10.00^\circ$, 22.40° , and 26.10° belonged to zeolite. These observations were in good agreement with the study of Xu et al. that synthesized $\text{TiO}_2/\text{ZnFe}_2\text{O}_4$ nanoparticles confirmed the peaks at $2\theta = 25.38^\circ$, 37.82° and 48.07° belonged to TiO_2 while diffraction peaks at $2\theta = 29.82^\circ$ and 35.24° were attributed to ZnFe_2O_4 compound [36]. The XRF results of $\text{N-TiO}_2/\text{ZnFe}_2\text{O}_4/\text{zeolite}$ (Table 3) revealed the amount of different elements of the catalyst and showed that the weight ratio of Al to Si for zeolite was 6.12 which was higher than 3.80 confirming the high thermal stability of the catalyst. The FT-IR spectra of FeZn_2O_4 , N-TiO_2 , $\text{N-TiO}_2/\text{ZnFe}_2\text{O}_4$, and $\text{N-TiO}_2/\text{ZnFe}_2\text{O}_4/\text{zeolite}$

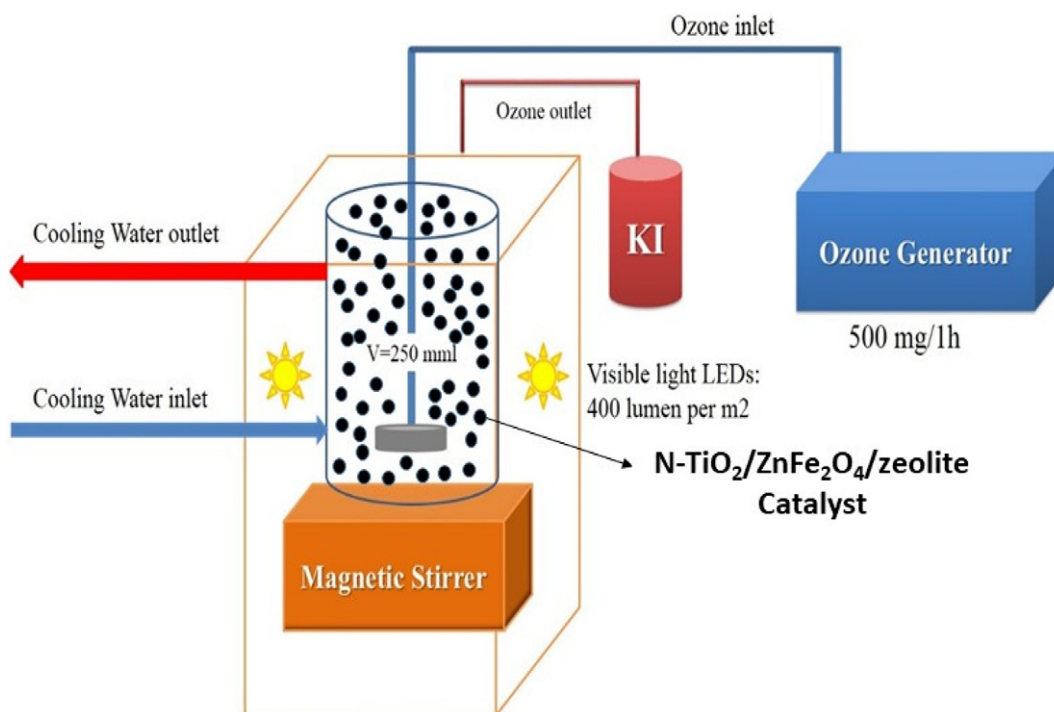


Fig. 2. The schematic of the photocatalytic reactor.

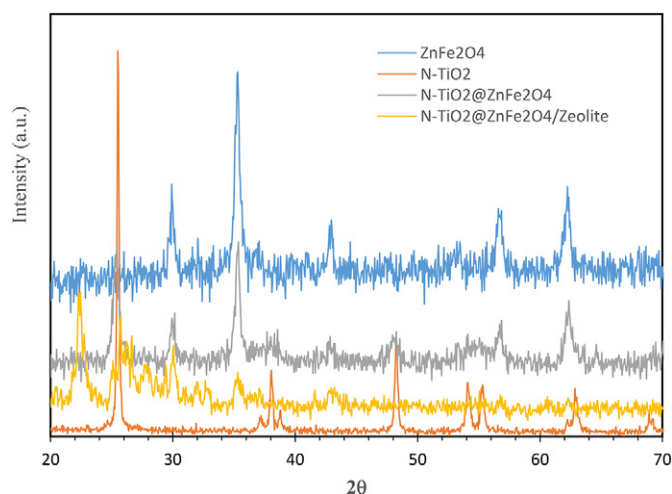


Fig. 3. XRD patterns of synthesized N-TiO₂, ZnFe₂O₄, N-TiO₂/ZnFe₂O₄/ and N-TiO₂/ZnFe₂O₄/zeolite.

ZnFe₂O₄ nanostructures were well distributed on the surface of zeolite. Similar results were reported in previous studies of synthesized N-TiO₂ and TiO₂/ZnFe₂O₄ confirming the presence of ZnFe₂O₄, TiO₂ and N in catalyst [42,55]. The results of UV-Vis DRS spectra (Fig. 6a) showed the effect of materials doping on the band gap energy. The adsorption edge of ZnFe₂O₄ was around 790 nm whereas the adsorption edges of N-TiO₂, N-TiO₂/ZnFe₂O₄, and N-TiO₂/ZnFe₂O₄/zeolite were 430, 530, and 590 nm, respectively. The results confirmed that the modification of TiO₂ with ZnFe₂O₄ led to a shift to the band gap energy of TiO₂ as the comparison of UV-Vis DRS spectrum of N-TiO₂ with that of N-TiO₂/ZnFe₂O₄, and N-TiO₂/ZnFe₂O₄/zeolite showed there was a shift to a longer wavelength and higher visible light absorption. Therefore, doping of nitrogen and ZnFe₂O₄ could play a crucial role in making TiO₂ catalyst active to photodegrade pollutants under visible light irradiation. This could be attributed to the formation of new energy storage centers between valence band (VB) and conduction band (CB) of TiO₂ [42]. The study of Yao et al. also showed a significant shift of the spectral response to around 550 nm for N-TiO₂/ZnFe₂O₄ compared to absorption edge of undoped TiO₂ which was at the UV region below 390 nm [42].

3.2. Model fitting and statistical analysis

The RSM models of second order polynomial equations were determined according to the results of experimental design obtained for each run. The quadratic models in terms of coded factors for metronidazole

Table 3
XRF results of N-TiO₂/ZnFe₂O₄/zeolite.

| Compound | Concentration (w/w%) |
|--------------------------------|----------------------|
| SiO ₂ | 55.82 |
| Al ₂ O ₃ | 9.37 |
| TiO ₂ | 5.86 |
| Fe ₂ O ₃ | 3.59 |
| CaO | 3.09 |
| Na ₂ O | 2.81 |
| BaO | 1.92 |
| SO ₃ | 1.19 |
| K ₂ O | 1.04 |
| ZnO | 1.015 |
| MgO | 0.464 |
| SrO | 0.271 |
| Cl | 0.235 |
| P ₂ O ₅ | 0.032 |
| CuO | 0.018 |
| ZrO ₂ | 0.018 |
| Total | 100.00 |

and cephalexin follow as Eqs. (3) and (4), respectively.

$$Y_{\text{MNZ}}(\%) = 83.51 - 2.72 * A + 3.66 * B + 3.93 * C - 6.25 * D + 0.095 * AB - 0.040 * AC - 0.43 * AD - 0.24 * BC + 0.23 * BD + 0.88 * CD - 0.79 * A^2 + 0.37 * B^2 + 2.41 * C^2 - 3.55 * D^2 \quad (3)$$

$$Y_{\text{CEX}}(\%) = 88.60 - 3.88 * A + 4.03 * B + 3.39 * C + 5.02 * D - 0.82 * AB - 1.11 * AC - 0.031 * AD + 0.42 * BC + 0.93 * BD + 0.049 * CD - 0.50 * A^2 + 0.80 * B^2 - 1.67 * C^2 - 18.68 * D^2 \quad (4)$$

The adequacy and significance of two models were evaluated by ANOVA results (Table 4) which showed the *F*-values for the models of metronidazole and cephalexin removal were 65.40 and 75.91, respectively confirming the models were highly significant. Besides, the *p*-values for both metronidazole and cephalexin removal were <0.0001 which further approved that the model terms were significant. The lack of fit value was 0.12 for metronidazole removal and 0.34 for cephalexin removal model. These results revealed the lack of fit of two models were not significant related to the pure error implying the good predictability of the fitted models around data variation. The determination coefficients *R*² of the quadratic regression model for the metronidazole removal was 0.984 and 0.986 for the cephalexin removal indicating that 98.4% and 98.6% of the variations for metronidazole and cephalexin degradation efficiency, respectively were explained by the independent variables. The adjusted *R*² values, which modified the *R*² values by considering the number of covariates or predictors in the model, were 0.969 and 0.973 for metronidazole and cephalexin, respectively. The close values of *R*² for both models with their adjusted values verified the predictability of both models and the high *R*² values implied the satisfactory adjustment of the quadratic models to the experimental data. Meanwhile, the adequate precision values for the metronidazole and cephalexin degradation efficiency were 34.46 and 27.93, respectively indicating remarkable signal (far >4).

The model and ANOVA results also provide information about the significance of the independent factors and their interaction according to *p*-value, *F*-value and coefficients of the quadratic model [28]. The results of metronidazole removal (Eq. (3) and Table 4) confirmed that although all four independent factors and the square pH had significant effects on the response (their *p*-value <<0.05), pH of the solution was the most vital factor on the metronidazole degradation efficiency as the *F*-value of pH and its coefficient value in Eq. (3) were much higher compared to other factors. There was no interaction between independent factors for the metronidazole removal as the *p*-values of all combination factors (AB, AC, AD, BC, BD, CD) were found to be >0.05 (Table 4). Further, the ANOVA results of cephalexin removal (Eq. (4) and Table 4) confirmed that the degradation efficiency was highly dependent on the level of pH and photocatalyst concentration in comparison with the cephalexin concentration and irradiation time. It also showed that there was an interaction between the cephalexin concentration and the irradiation time. Moreover, the positive coefficients of the quadratic models imply their positive effects on the response whereas the negative ones indicate their negative roles on the degradation efficiency. Consequently, increasing the pH and metronidazole concentration or reduction of irradiation time as well as photocatalyst concentration could act as a deterrent to the performance enhancement of metronidazole removal. In the case of cephalexin removal, increasing pH to neutral pH and increasing other factors except the pollutant concentration could improve the cephalexin degradation efficiency.

3.3. Effect of processing factors and optimization

The effect of catalyst and pollutants concentration on the response is shown in Fig. 7a. The degradation efficiency for both metronidazole and

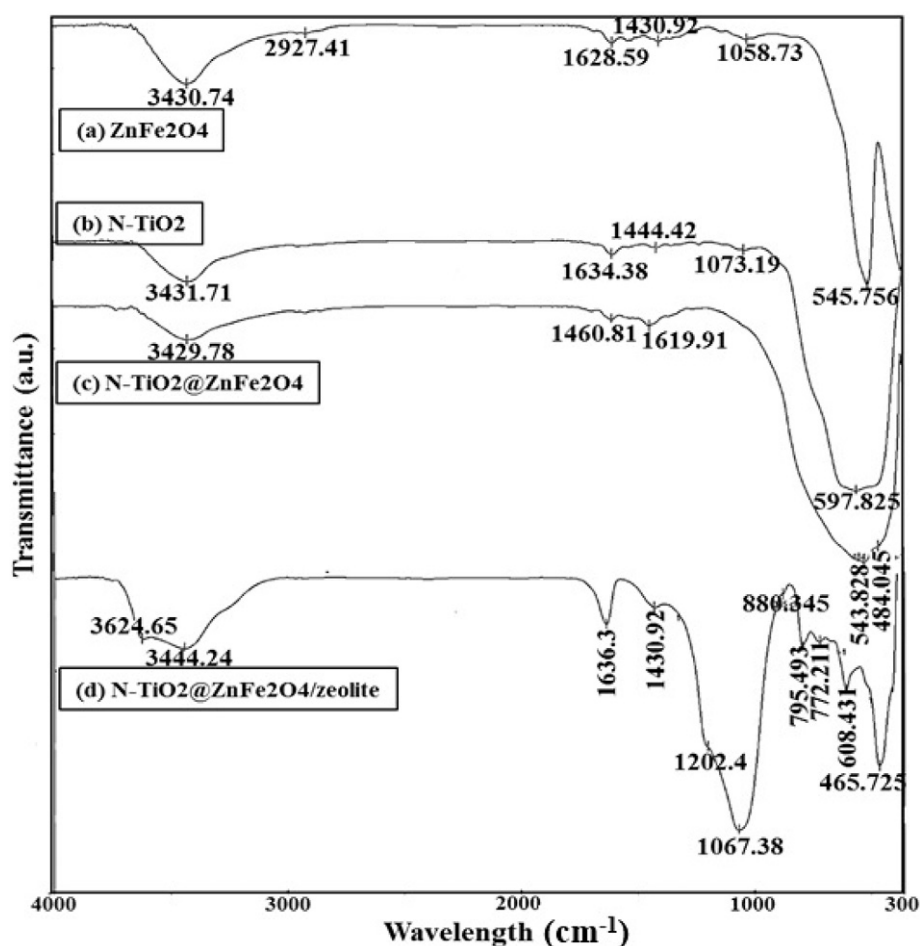


Fig. 4. FTIR spectra of (a) FeZn₂O₄, (b) N-TiO₂, (c) N-TiO₂/ZnFe₂O₄, and (d) N-TiO₂/ZnFe₂O₄/zeolite.

cephalexin removal decreased to 75% and 82%, respectively with an increase in pollutants concentration from 10 mg/L to 100 mg/L. Such reduction trends can be explained with the fact that when the concentration of metronidazole or cephalexin is low, more available active sites of the photocatalyst exist as compared with the pollutant molecules which leads to easy adsorption of the contaminant molecules on the surface of the catalyst and thereby easy interaction of pollutant molecules with the generated hydroxyl radicals. However, the number of active sites is far lower than the pollutant molecules at the higher concentration of metronidazole or cephalexin. Therefore, the lack of adsorption sites at the higher pollutants concentration makes the interaction of pollutants and hydroxyl radicals difficult and also leads to the lower adsorption of the contaminant molecules which these unadsorbed molecules cause lower penetration of photons through the solution and the reduction of degradation efficiency. Besides, these plots also evaluated the trend of degradation efficiency with increasing the concentration of N-TiO₂/ZnFe₂O₄/zeolite nanoparticles. The plots revealed that there was an upward trend for the degradation efficiency of both metronidazole and cephalexin with increasing the catalyst concentration. Increasing the catalyst concentration from 1 to 2 g/L contributed to the increase of the degradation efficiency from 79% to 91% and from 85% to 95% for the metronidazole and cephalexin removal, respectively, which confirmed that N-TiO₂/ZnFe₂O₄/zeolite compound had high potential to degrade pollutants, especially antibiotics. This ascending trend could be attributed to the light penetration of photoactivating light into the suspension and an increase in the number of active sites and photon absorbed and thereby contributing to the generation of more hydroxyl radicals and enhancement of the degradation efficiency.

The plot of the degradation efficiency as a function of pH (Fig. 7b) indicated that the metronidazole degradation efficiency was achieved almost 91% at pH 4 followed by a significant decrease of about 25% under alkaline condition (pH = 10). However, the cephalexin degradation efficiency experienced a different trend with an increase in the pH as it increased from 65% to 92% with increasing the pH from 4 to 7 and then it declined to around 79% with increasing pH to 10. These trends can be justified by pHzpc of the catalyst and pKa of the metronidazole and cephalexin. The pHzpc of the N-TiO₂/ZnFe₂O₄/zeolite is 7.4 that means the surface of the catalyst has negative charge at pH > pHzpc. The pKa of metronidazole is 2.5 so that at higher pH than 2.5 the metronidazole is in anionic form. Therefore, the remarkable drop of metronidazole degradation efficiency at pH of 10 is owing to the electrostatic repulsion between the photocatalyst surface and the metronidazole molecules which has a negative effect on the adsorption of pollutant on the surface of N-TiO₂/ZnFe₂O₄/zeolite nanostructure. Moreover, in the case of cephalexin the pKa has two different values as for the carboxyl group its value is 2.6 and pKa = 6.9 for the amine group [14]. Therefore, at the pH lower than 2.6 the cephalexin molecule is positively charged and in the range of 2.6 to 6.9, cephalexin is in zwitterionic form while at pH higher than 6.9 it is negatively charged [14]. Besides, the hydrophobic property of cephalexin is dependent on the pH of solution because cephalexin is a zwitterion, i.e. the molecule contains both a basic and an acidic group [17]. In the pH range of 4 to 7, cephalexin exists in higher concentrations at the bubble surface and thus it has high potential to be degraded by hydroxyl radicals [17]. However, at pH of 10, because cephalexin is in anionic form the hydrophilicity and solubility of cephalexin are improved and the degradation is occurred in the bulk of the solution

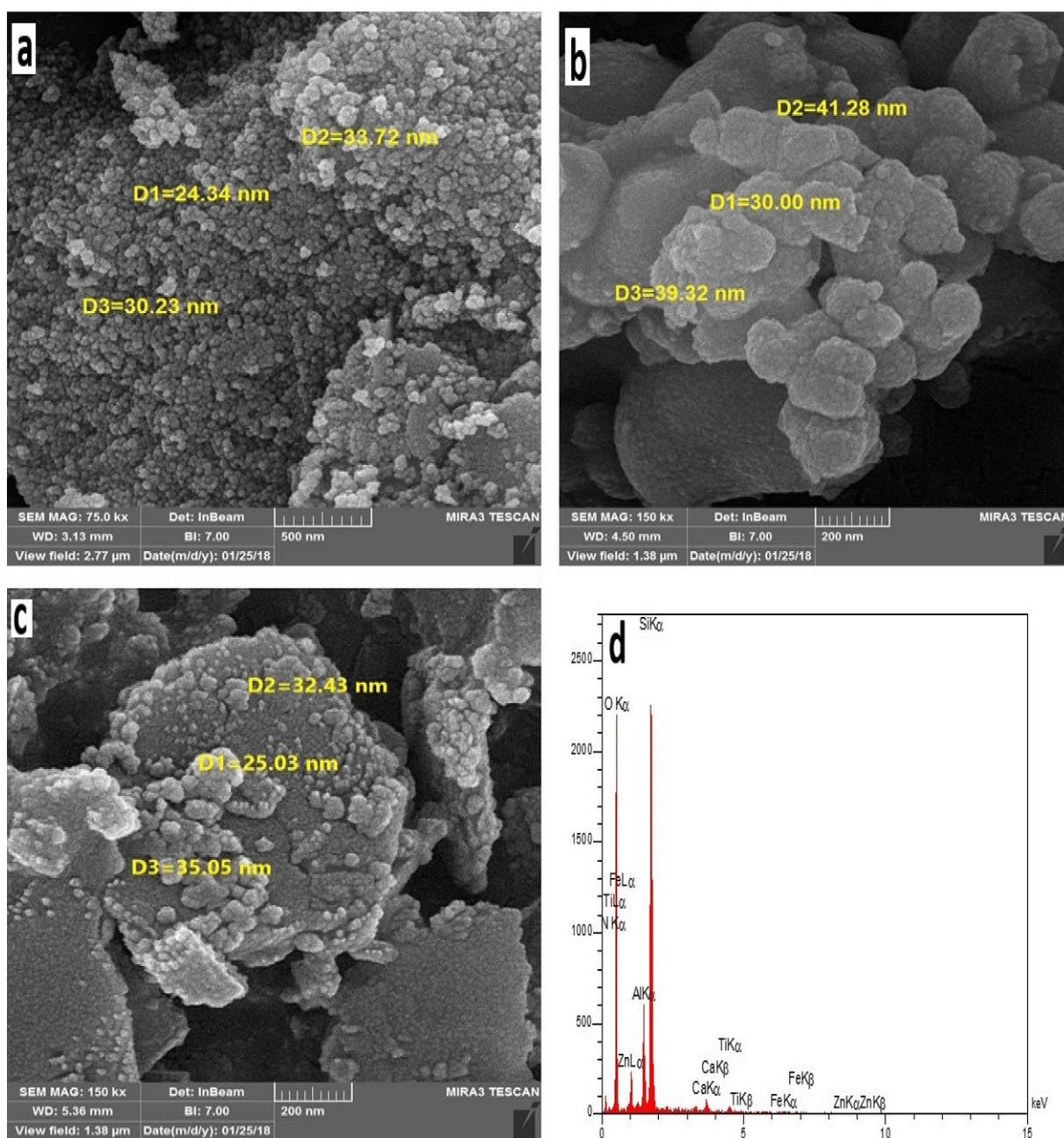


Fig. 5. FE-SEM images of (a) FeZn₂O₄, (b) N-TiO₂, (c) N-TiO₂/ZnFe₂O₄/zeolite, and (d) EDX spectrum of N-TiO₂/ZnFe₂O₄/zeolite.

where, there is a lower concentration of hydroxyl radicals and hence, the degradation efficiency decreases [17]. Another reason for the reduction of degradation efficiency at pH of 10 is due to the repulsive forces between cephalixin in anionic form and negative charge of N-TiO₂/ZnFe₂O₄/zeolite catalyst surface avoiding reaching the cephalixin molecules near the produced hydroxyl radicals on the surface of the catalyst [14].

The trend of photocatalytic degradation efficiency of pollutants as a function of irradiation time is shown in Fig. 7c. The metronidazole and cephalixin degradation efficiencies enhanced to 90% and 94%, respectively by increasing the visible light irradiation time from 60 min to 120 min. The increasing of irradiation time contributes to more time for the generation of hydroxyl radicals which increases the number of generated hydroxyl radicals. Besides, increasing of the irradiation time means that there is more reaction time between the pollutants and

produced hydroxyl radicals which leads to the more degradation of antibiotics.

The optimum conditions of the independent variables to achieve maximum antibiotic degradation efficiency were determined using the desirability function ranked in the range of 0 to 1. The higher desirability implies the more desirable set of optimum conditions. The maximum metronidazole efficiency using Box-Behnken design at desirability of 1 was predicted 95.6% under the optimum conditions of metronidazole concentration of 100 mg/L, pH of 5, catalyst concentration of 2 g/L and 120 min visible light irradiation time whereas the model predicted that 96.1% of cephalixin was degraded by following the values of process conditions: 100 mg/L of initial cephalixin concentration, pH = 7, the N-TiO₂/ZnFe₂O₄/zeolite concentration of 2 g/L and 120 min irradiation time. The experimental results of metronidazole and cephalixin degradation under the optimum conditions revealed

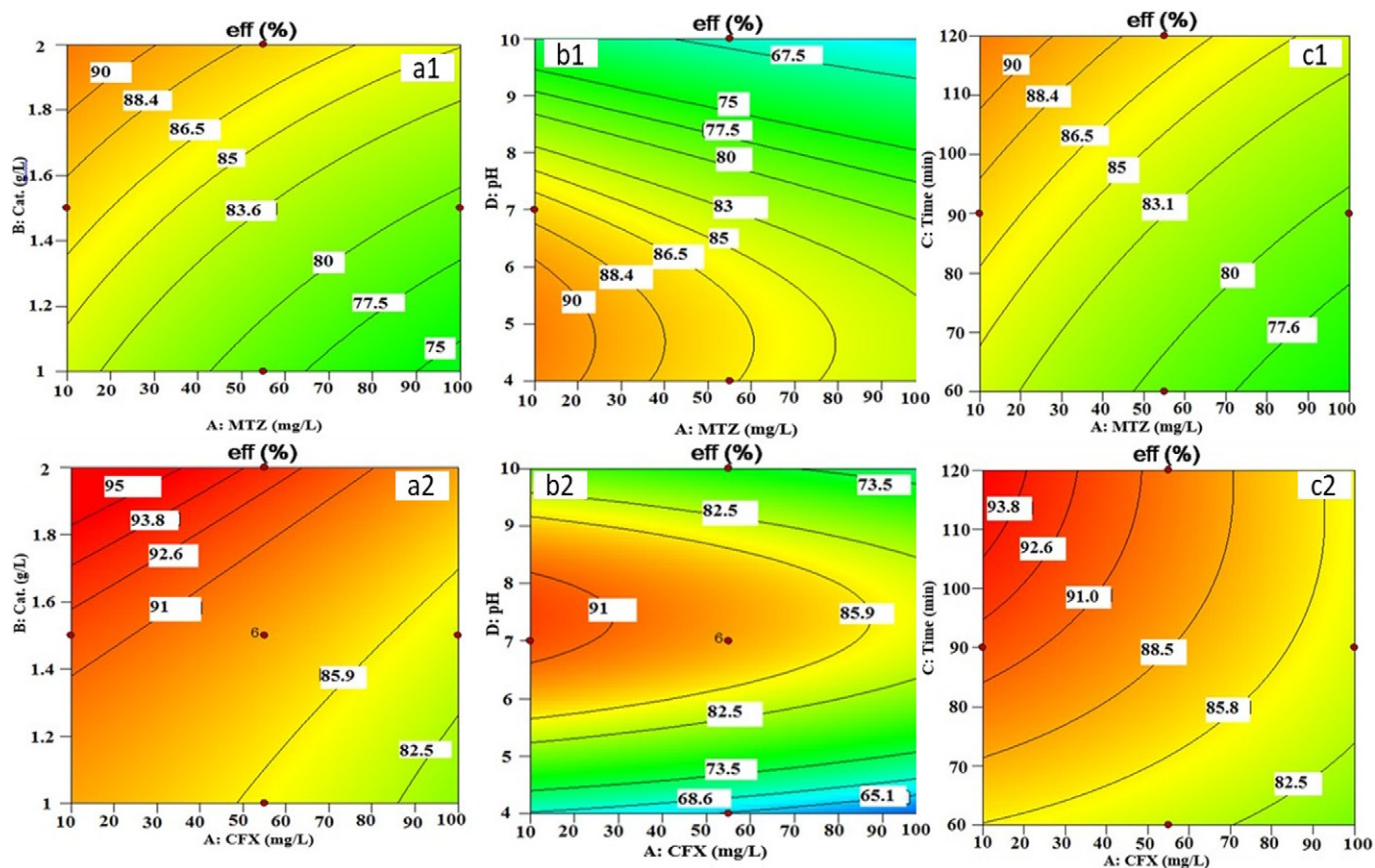


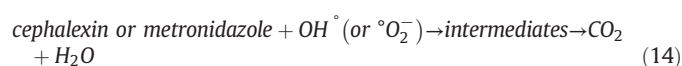
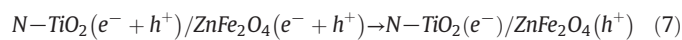
Fig. 7. The plots of antibiotics removal efficiency versus a) initial pollutant concentration and catalyst concentration b) pH and c) irradiation time, a1,b1,c1 for metronidazole and a2,b2,c2 for cephalixin.

cephalexin than metronidazole. This could be due to difference in the structure of two pollutants.

3.4. The mechanisms of photocatalytic ozonation degradation, effects of different processes of antibiotics removal and the effect of N:TiO₂ and N-TiO₂:ZnFe₂O₄ weight ratio

The mechanism of photocatalytic degradation of N-TiO₂/ZnFe₂O₄/zeolite nanoparticles under visible light irradiation combined with ozonation process is shown in Fig. 8. The photocatalytic oxidation mechanism is based on the electrons in the valence band (VB) and holes in the conduction band (CB) formed upon the light exposure. ZnFe₂O₄ with narrow band gap energy (1.9 eV) [36] has high potential to be easily excited under visible light irradiation from VB to CB which leads to the generation of electron-hole pairs [42]. Besides, the band gap of TiO₂ is reduced by N doping and hence N-TiO₂ can be excited under visible light. However, for the N-TiO₂/ZnFe₂O₄/zeolite photocatalyst, the photogenerated electrons can transfer from the VB of ZnFe₂O₄ to the CB of N-TiO₂ because the potential of conduction band of N-TiO₂ is more positive as compared to that of the ZnFe₂O₄ band [36,42]. This contributes to formation of the positive hole (h⁺) in the VB of ZnFe₂O₄ enhancing the transfer of photogenerated charge carriers (Eqs. (6) and (7)). Therefore, electron-hole pairs are more likely to be effectively separated and the recombination of electron-hole pairs decreases which in turn improves the photocatalytic activity. The photogenerated electrons and holes produced by ZnFe₂O₄ and N-TiO₂ can react with O₂ and H₂O and generate the reactive oxygen species ([•]O₂⁻, [•]OH) (Eqs. (8)–(10)) [36]. Furthermore, the combination of photocatalysis degradation with ozonation process can also play a vital role in increasing the generation of reactive species, such as hydroxyl radicals, as a result of the electron transfer from N-TiO₂ to the

ozone molecule (Eqs. (11)–(13)) [43]. These oxygen reactive species can react with antibiotics and degrade metronidazole and cephalixin to harmless materials (Eq. (14)).



The effects of different processes of the cephalixin and metronidazole removal including adsorption removal, ozonation process, photolysis degradation method and photocatalysis process or combination of such methods were appraised (Table 5). The results of adsorption removal on metronidazole and cephalixin removal at the optimum conditions using N-TiO₂/ZnFe₂O₄/zeolite as an adsorbent showed the adsorption removal efficiencies of metronidazole and cephalixin were

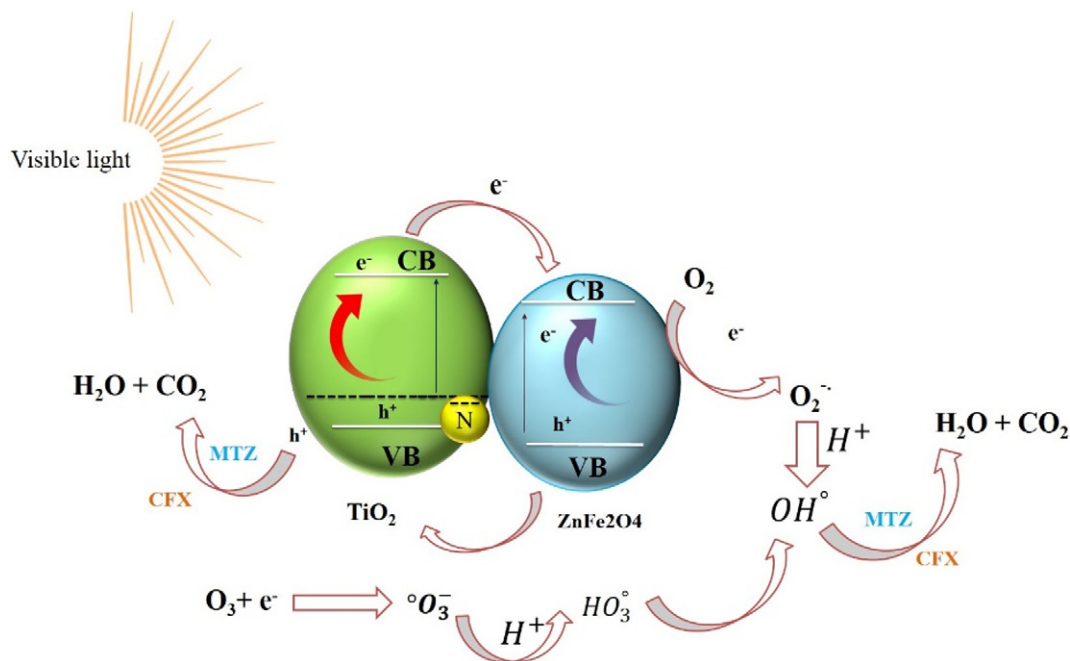


Fig. 8. Possible photocatalytic ozonation mechanism of N-TiO₂/ZnFe₂O₄/zeolite composite under visible light irradiation for metronidazole and cephalixin degradation.

11% and 14%, respectively, which were relatively negligible. The degradation efficiency of antibiotics by photolysis method (using UV-vis alone) was also insignificant (4% metronidazole and 5% cephalixin). The results showed the degradation efficiencies of ozonation process for the metronidazole and cephalixin removal were obtained 36% and 39%, respectively, whereas the combination of ozonation and photolysis processes (O₃/UV-vis) improved the photodegradation performance (43% metronidazole, 46% cephalixin). It can be attributed to the elevated amount of hydroxyl radicals (Eqs. (11)–(13)). The photocatalytic activity of N-TiO₂/ZnFe₂O₄/zeolite under UV-vis irradiation was determined 70% for metronidazole and 74% for cephalixin degradation. Furthermore, the combination of ozonation process and photocatalytic degradation under visible light irradiation (N-TiO₂/ZnFe₂O₄/zeolite/

O₃/UV-vis) showed high potential for the antibiotics degradation (94% for metronidazole and 95% for cephalixin) due to the increase in the generation of reactive species (Eqs. (6)–(13)) and synergistic effects between photocatalysis and ozonation processes.

Moreover, Table 5 lists the degradation efficiencies of various types of AOPs for CEX and MNZ removal including UV, H₂O₂, O₃, O₃/UV, UV/H₂O₂, UV/O₃/catalyst, and UV/H₂O₂/catalyst to compare the performance of photocatalytic ozonation process using N-TiO₂/ZnFe₂O₄/zeolite as a photocatalyst under visible light irradiation with other related studies taken under evaluation in previous works. The results exhibited the excellent photocatalytic ozonation activity of the process applied in this study for the degradation of antibiotics. Comparison the removal efficiency of MNZ and CEX showed that using N-TiO₂/ZnFe₂O₄/zeolite/O₃/

Table 5

Comparison the performance of different types of AOPs for MNZ and CEX removal.

| Process type | Optimum conditions | Efficiency (%) | References |
|--|--|----------------|------------|
| UV-vis | [MNZ] = 100 mg/L, pH = 5, Time = 120 min | 4 | This study |
| Ozonation | [MNZ] = 100 mg/L, pH = 5, Time = 120 min, O ₃ = 500 mg/h | 36 | This study |
| O ₃ /UV-vis | [MNZ] = 100 mg/L, pH = 5, Time = 120 min, O ₃ = 500 mg/h | 43 | This study |
| N-TiO ₂ /ZnFe ₂ O ₄ /zeolite/UV-vis | [MNZ] = 100 mg/L, pH = 5, [catalyst] = 2 g/L, Time = 120 min | 70 | This study |
| N-TiO ₂ /ZnFe ₂ O ₄ /zeolite/O ₃ /UV-vis | [MNZ] = 100 mg/L, pH = 5, [catalyst] = 2 g/L, Time = 120 min, O ₃ = 500 mg/h | 94 | This study |
| Ozonation | [MNZ] = 20 mg/L, pH = 11, reaction time = 30 min | 55 | [15] |
| Ozonation with ZnO | [MNZ] = 20 mg/L, pH = 11, catalyst dosage = 2 g/L, and reaction time = 30 min | 77 | [15] |
| ZnO/Fe ₂ O ₃ /Clinoptilolite/UV/H ₂ O ₂ | [MNZ] = 60 mg/L, Time = 90 min, [catalyst] = 1 g/L pH = 10, [H ₂ O ₂] = 40 mg/L | 99 | [57] |
| ZnO/Fe ₂ O ₃ /Clinoptilolite/H ₂ O ₂ | [MNZ] = 60 mg/L, Time = 90 min, pH = 10, [catalyst] = 1 g/L, [H ₂ O ₂] = 40 mg/L | 40 | [57] |
| ZnO/Fe ₂ O ₃ /Clinoptilolite/UV | [MNZ] = 60 mg/L, Time = 90 min, [catalyst] = 1 g/L pH = 10 | 95 | [57] |
| UV/H ₂ O ₂ | [MNZ] = 60 mg/L, Time = 90 min, pH = 10, [H ₂ O ₂] = 40 mg/L | 25 | [57] |
| H ₂ O ₂ | [MNZ] = 60 mg/L, Time = 90 min, pH = 10, [H ₂ O ₂] = 40 mg/L | 10 | [57] |
| UV-vis | [CEX] = 100 mg/L, pH = 7, Time = 120 min | 5 | This study |
| Ozonation | [CEX] = 100 mg/L, pH = 7, Time = 120 min, O ₃ = 500 mg/h, | 39 | This study |
| O ₃ /UV-vis | [CEX] = 100 mg/L, pH = 7, Time = 120 min, O ₃ = 500 mg/h | 46 | This study |
| N-TiO ₂ /ZnFe ₂ O ₄ /zeolite/UV-vis | [CEX] = 100 mg/L, pH = 7, [catalyst] = 2 g/L, Time = 120 min | 74 | This study |
| N-TiO ₂ /ZnFe ₂ O ₄ /zeolite/O ₃ /UV-vis | [CEX] = 100 mg/L, pH = 7, [catalyst] = 2 g/L, Time = 120 min, O ₃ = 500 mg/h | 95 | This study |
| Sono-Fenton | [CEX] = 50 mg/L, pH = 3, [H ₂ O ₂] = 60 mg/L, [Fe ²⁺] = 8 mg/L, Time = 60 min | 90 | [58] |
| ZnO/UV | [CEX] = 5 mg/L, [ZnO] = 2 g/L, pH = 7, Time = 45 min radiation Intensity = 18 W | 81.8 | [59] |
| TiO ₂ /UV | [CEX] = 5 mg/L, [TiO ₂] = 2 g/L pH = 7, Time = 45 min radiation Intensity = 18 W | 63.5 | [59] |
| Photolysis (UV) | [CEX] = 50 mg/L, pH = 6, Time = 120 min | 8.73 | [60] |
| TiO ₂ /UV/H ₂ O ₂ | [CEX] = 50 mg/L, pH = 6, [TiO ₂] = 1 g/L, H ₂ O ₂ = 0.15 mL, Time = 120 min | 93.47 | [60] |
| US/H ₂ O ₂ /NiO | [CEX] = 40 mg/L, pH = 3, [NiO] = 7.5 mg/L, H ₂ O ₂ = 30 mL/L, Time = 90 min | 93.86 | [61] |

UV-vis process had high potential to treat wastewaters contained pharmaceutical compounds even at high initial concentration of antibiotics (100 mg/L) and this can be a superiority of this study compared to others listed in Table 5 as other studies were able to remove antibiotics with lower initial antibiotic concentration (maximum 60 mg/L). Further, these studies showed that UV or H_2O_2 as an individual process of wastewater purifications was inefficient in decomposition of MNZ and CEX and their removal efficiencies were <10%, which were much lower as compared to the ozonation process with removal efficiencies in the range of 36–55%. This is due to higher oxidation–reduction potential of ozone (2.07 eV) than H_2O_2 (1.77 eV) and its ability to decompose contaminants by both direct ozonation and indirect use of hydroxyl radicals (2.85 eV). Meanwhile, the modification of ozone with H_2O_2 or UV (O_3/H_2O_2 and O_3/UV) showed much higher activity for antibiotic decomposition than UV/ H_2O_2 . Further, Table 5 verified that a novel visible-light responsive N-TiO₂/ZnFe₂O₄/zeolite can be a potential nanocatalyst for degradation of contaminants compared to some other catalysts investigated in previous studies. In general, considering the role of ozone injection as well as photocatalytic activity of N-TiO₂/ZnFe₂O₄/zeolite nanostructure which lead to high removal efficiency even at high pollutant concentration with low consumption of catalyst,

photocatalytic ozonation process can be more beneficial for wastewater treatment than other types of AOPs.

The performance of N-TiO₂ catalyst with and without the presence of zeolite and ZnFe₂O₄ on photocatalytic degradation was also assessed. The results indicated that the efficiency of both cephalexin and metronidazole improved markedly when TiO₂ was modified by N and ZnFe₂O₄ as the efficiency of N-TiO₂/ZnFe₂O₄ was obtained 70% and around 80% for metronidazole and cephalexin removal respectively (Fig. 9). These were far more than the efficiencies of N-TiO₂ (50–60%), bare ZnFe₂O₄ (30–40%) and TiO₂/ZnFe₂O₄ (70–75%) because impregnation of the TiO₂ semiconductor using N and ZnFe₂O₄ leads to the changes in the band gap energy and the absorption edge playing a vital role in the generation of reactive species, especially hydroxyl radicals (Eqs. (6)–(10)) and thereby enhancing the photodegradation efficiency. While the bare ZnFe₂O₄ has low performance to degrade pollutants because of its lower valance band potential and poor property in photoelectric conversion, it could be an appropriate option for doping with TiO₂ due to its sensitivity to visible light and no photochemical corrosion property [56]. Besides, the comparison of the photocatalytic activity of N-TiO₂/ZnFe₂O₄ (83–89%) and N-TiO₂/ZnFe₂O₄/zeolite (94–95%) confirmed that not only using zeolite as a support could have positive effects on boosting

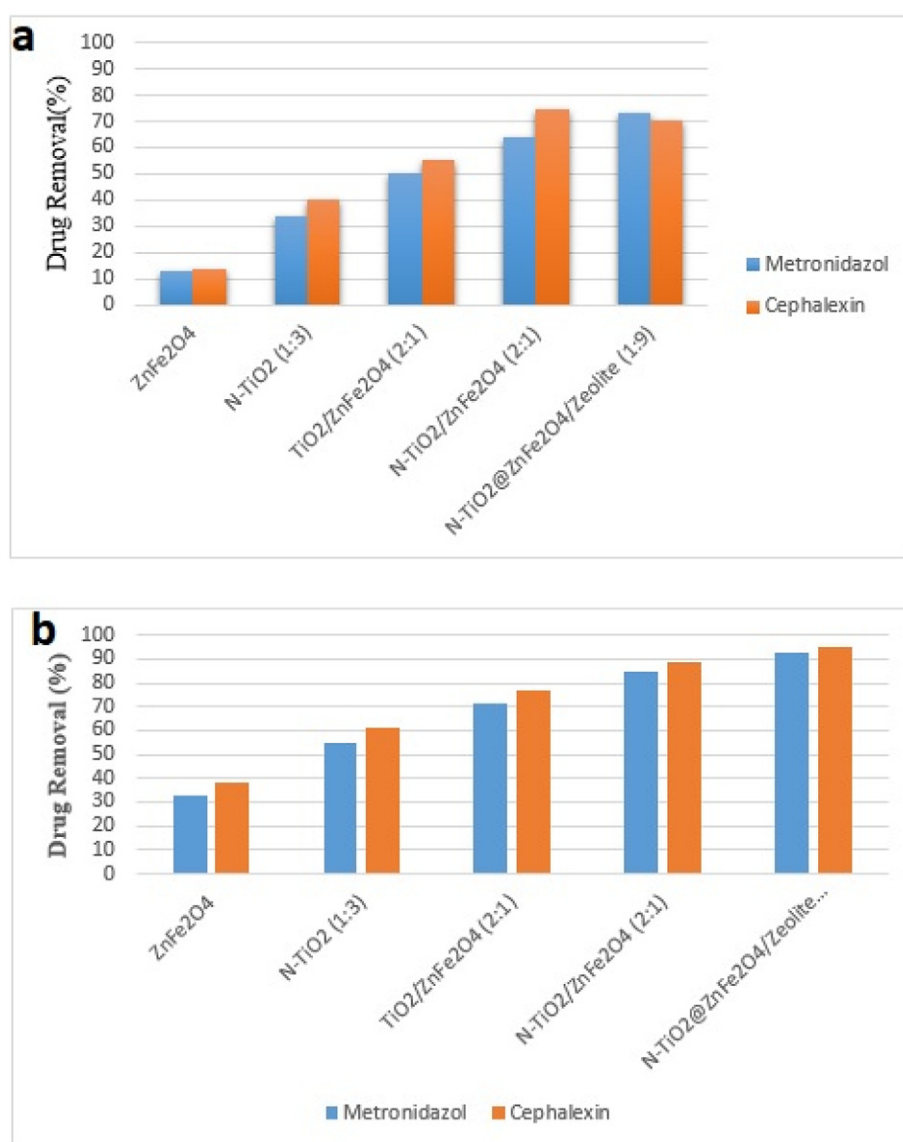


Fig. 9. Effects of ZnFe₂O₄, N-TiO₂, N-TiO₂/ZnFe₂O₄ and N-TiO₂/ZnFe₂O₄/zeolite for metronidazole and cephalexin a) photodegradation b) ozonation and photodegradation.

the photodegradation efficiency but also it could make the nanoparticle as a reusable catalyst.

The effect of N: TiO₂ weight ratio on the photodegradation efficiency of both metronidazole and cephalixin at the optimum conditions with and without the presence of ozone was investigated. An increase in the weight ratio of N: TiO₂ from 0.5:3 to 1:3 resulted in a slight increase in the metronidazole removal from 25% to 34%, respectively, whereas a downward trend was observed with further increase of the weight ratio to 1.5:3. The cephalixin photocatalyst degradation also experienced similar trends as its photodegradation efficiency was obtained 30% at the N:TiO₂ weight ratio of 0.5:3 and it peaked at 40% for the weight ratio of 1:3, followed by a decrease to 34% at weight ratio of 1.5:3. Increasing the weight ratio of N: TiO₂ causes the enhancement of the number of nitrogen atoms which replaces the oxygen sites atoms contributing to an increase of oxygen vacancy and Ti³⁺ and thereby enhancing the photocatalytic activity of N-TiO₂ and boosting the degradation efficiency. However, further increase of the N: TiO₂ weight ratio can have negative effects on the enhancement of the degradation efficiency because oxygen vacancies and Ti³⁺ sites can become the recombination centers at higher weight ratios which in turn can reduce the photocatalytic efficiency. Meanwhile, the bare TiO₂ without doping of nitrogen had low photocatalytic activity to degrade antibiotics under visible light irradiation (around 14–15% for both pollutants). This can be attributed to the wide band gap of TiO₂ which is inactive under visible light irradiation and hence has low degradation efficiency. Moreover, the optimum weight ratio of N-TiO₂: ZnFe₂O₄ to obtain the maximum degradation efficiency was also determined. The results confirmed increasing the N-TiO₂:ZnFe₂O₄ weight ratio from 1:1 to 2:1 increased the degradation efficiency of metronidazole and cephalixin to 64% and 75%, respectively followed by a decline to 52% and 68% for the metronidazole and cephalixin removal, respectively by further increasing the N-TiO₂:ZnFe₂O₄ weight ratio to 3:1. The upward trend of the degradation efficiency of both antibiotics could be due to increase in the number of active sites, the photocatalytic reaction centers and hydroxyl radicals with increasing the N-TiO₂:ZnFe₂O₄ weight ratio to 2:1. Nevertheless, at higher N-TiO₂:ZnFe₂O₄ weight ratio, due to the role of ZnFe₂O₄ as electron-hole recombination centers, the photocatalytic activity reduces. Moreover, the results also verified that N-TiO₂ without doping of ZnFe₂O₄ had the lowest degradation efficiency for both antibiotics as compared to N-TiO₂/ZnFe₂O₄ with different weight ratios of N-TiO₂:ZnFe₂O₄. This could be justified by the PL emission spectral results of N-TiO₂ and N-TiO₂/ZnFe₂O₄ (Fig. 6b). The emission peak for both photocatalyst was around 530 nm. Since the PL emission is the result of charge carrier recombination, the lower PL intensity represents the lower photogenerated electron-hole recombination rate [28]. The lower intensity of N-TiO₂/ZnFe₂O₄ compared to that of N-TiO₂ shows a better charge separation and higher photocatalytic activity of N-TiO₂/ZnFe₂O₄ than N-TiO₂. Consequently, doping of ZnFe₂O₄ on the surface of N-TiO₂ leads to a more efficient charge separation, prolonging the lifetime of the charge carriers, and thereby improving the interfacial charge transfer efficiency and enhancing the performance of photocatalytic activity.

4. Conclusion

The performance of N-TiO₂/ZnFe₂O₄/zeolite compound in the photocatalytic ozonation process under visible light irradiation improved greatly as >90% of cephalixin and metronidazole degraded even after four times of catalyst and the removal efficiency was highly dependent on the weight ratio of N:TiO₂ and N-TiO₂:ZnFe₂O₄. The results of response surface methodology and experimental design exhibited high R² values, high F-values, very low p-values, and nonsignificant lack of fit values confirming good agreement between the experimental and predicted values of the response for both pollutants removal. The first order kinetic study confirmed that N-TiO₂/ZnFe₂O₄/zeolite/O₃ under visible light irradiation system was more effective to degrade

cephalexin than metronidazole as the degradation rate of cephalixin was 1.2 times higher than that of metronidazole. In general, based on the findings, using the reusable N-TiO₂/ZnFe₂O₄/zeolite compound as a high visible-light active catalyst and the combination of photocatalytic degradation and ozonation processes and also O₃-based AOPs are suggested for the water treatment process.

Acknowledgement

The authors gratefully acknowledge the Iranian National Nanotechnology and the Environmental Research Institute - University of Isfahan, Initiative for the scientific assistance in the respect.

References

- [1] D. Kanakaraju, B.D. Glass, M. Oelgemöller, *J. Environ. Manag.* 219 (2018) 189.
- [2] N. Davari, M. Farhadian, A.R. Solaimany Nazar, M. Homayounfal, *J. Environ. Chem. Eng.* 5 (2017) 5707.
- [3] M.B. Johnson, M. Mehrvar, *Ind. Eng. Chem. Res.* 47 (2008) 6525.
- [4] J. Rivera-Utrilla, M. Sánchez-Polo, M.Á. Ferro-García, G. Prados-Joya, R. Ocampo-Pérez, *Chemosphere* 93 (2013) 1268.
- [5] Y. Lan, C. Coetsier, C. Causserand, K.G. Serrano, *Chem. Eng. J.* 333 (2018) 486.
- [6] S. Ramanayaka, B. Sarkar, A.T. Cooray, Y.S. Ok, M. Vithanage, *J. Hazard. Mater.* 384 (2020), 121301.
- [7] N. Ajoudanian, A. Nezamzadeh-Ejhi, *Mater. Sci. Semicond. Process.* 36 (2015) 162.
- [8] L. Xu, W. Li, P. Désèsquelles, N.-T. Van-Oanh, S. Thomas, J. Yang, *J. Phys. Chem. A* 123 (2019) 933–942.
- [9] B. Karimi, M.H. Habibi, *J. Ind. Eng. Chem.* 80 (2019) 292–300.
- [10] J. He, Y. Zhang, Y. Guo, G. Rhodes, J. Yeom, H. Li, Z. Wei, *Environ. Int.* 132 (2019), 105105.
- [11] H. Wu, Q. Feng, H. Yang, E. Alam, B. Gao, D. Gu, *Colloids Surf. A Physicochem. Eng. Asp.* 517 (2017) 63.
- [12] N. Neghi, M. Kumar, D. Burkhalov, *Chem. Eng. J.* 359 (2019) 963.
- [13] X. Hu, J. Fan, K. Zhang, N. Yu, J. Wang, *Ind. Eng. Chem. Res.* 53 (2014) 14623.
- [14] F. Toriki, H. Faghhihian, *J. Photochem. Photobiol. A Chem.* 338 (2017) 49.
- [15] N. Nasseh, F.S. Arghavan, S. Rodriguez-Couto, A.H. Panahi, M. Esmati, T.J. A-Musawi, *Adv. Powder Technol.* (2019).
- [16] W. Cheng, M. Yang, Y. Xie, B. Liang, Z. Fang, E.P. Tsang, *Chem. Eng. J.* 220 (2013) 214.
- [17] W. Guo, H. Wang, Y. Shi, G. Zhang, *Water SA* 36 (2010).
- [18] D.A. Coledam, M.M.S. Pupo, B.F. Silva, A.J. Silva, K.I.B. Eguiluz, G.R. Salazar-Banda, J.M. Aquino, *Chemosphere* 168 (2017) 638.
- [19] S. Azimi, A. Nezamzadeh-Ejhi, *J. Mol. Catal. A Chem.* 408 (2015) 152.
- [20] A. Maleki, F. Moradi, B. Shahmoradi, R. Rezaee, S.-M. Lee, *J. Mol. Liq.* 297 (2019), 111918.
- [21] S.J. Baloochi, A.R.S. Nazar, M. Farhadian, *Environ. Nanotechnol. Monit. Manag.* 10 (2018) 212.
- [22] E.M. Cuerda-Correa, M.F. Alexandre-Franco, C. Fernández-González, *Water* 12 (2020) 102.
- [23] A.K. Biñ, S. Sobera-Madej, *Ozone Sci. Eng.* 34 (2012) 136.
- [24] H. Suzuki, S. Araki, H. Yamamoto, *J. Water Proc. Eng.* 7 (2015) 54.
- [25] Y. Zeng, D. Chen, T. Chen, M. Cai, Q. Zhang, Z. Xie, R. Li, Z. Xiao, G. Liu, W. Lv, *Chemosphere* 227 (2019) 198.
- [26] B. Li, C. Lai, G. Zeng, L. Qin, H. Yi, D. Huang, C. Zhou, X. Liu, M. Cheng, P. Xu, *ACS Appl. Mater. Interfaces* 10 (2018) 18824.
- [27] P. Eskandari, M. Farhadian, A.R. Solaimany Nazar, B.-H. Jeon, *Ind. Eng. Chem. Res.* 58 (5) (2019) 2099–2112.
- [28] J.-H. Tzeng, C.-H. Weng, Y.-H. Lin, S.-M. Huang, L.-T. Yen, J. Anotai, Y.-T. Lin, *J. Ind. Eng. Chem.* 80 (2019) 376–384.
- [29] N. Adnen, M. Abdullah, M. Nor, *IOP Conference Series: Materials Science and Engineering*, IOP Publishing, 2018 012020.
- [30] J. Nowotny, M.A. Alim, T. Bak, M.A. Idris, M. Ionescu, K. Prince, M.Z. Sahdan, K. Sopian, M.A.M. Teridi, W. Sigmund, *Chem. Soc. Rev.* 44 (2015) 8424.
- [31] H. Zangeneh, A.A. Zinatizadeh, S. Zinatini, *Sep. Purif. Technol.* (2020) 116591.
- [32] T. Suwannaruang, K. Kamonsuangkasem, P. Kidkhunthod, P. Chirawatkul, C. Saiyasombat, N. Chanlek, K. Wantala, *Mater. Res. Bull.* 105 (2018) 265.
- [33] J. Prakash, P. Kumar, R. Harris, C. Swart, J. Neethling, A.J. van Vuuren, H. Swart, *Nanotechnology* 27 (2016), 355707.
- [34] F. Toriki, H. Faghhihian, *RSC Adv.* 7 (2017), 54651.
- [35] Q. Xu, J. Feng, L. Li, Q. Xiao, J. Wang, *J. Alloys Compd.* 641 (2015) 110.
- [36] A.-A. Salarian, Z. Hami, N. Mirzaei, S.M. Mohseni, A. Asadi, H. Bahrami, M. Vosoughi, A. Alinejad, M.-R. Zare, *J. Mol. Liq.* 220 (2016) 183.
- [37] Z. Yu, H. Moussa, B. Chouchene, M. Liu, R. Schneider, W. Wang, M. Molieri, H. Liao, *Nanotechnology* 30 (2018) 045707.
- [38] E. Casbeer, V.K. Sharma, X.-Z. Li, *Sep. Purif. Technol.* 87 (2012) 1.
- [39] Y. Hou, X. Li, Q. Zhao, X. Quan, G. Chen, *Environ. Sci. Technol.* 44 (2010) 5098.
- [40] L.G. Devi, R. Kavitha, *RSC Adv.* 4 (2014), 28265.
- [41] Y. Yao, J. Qin, H. Chen, F. Wei, X. Liu, J. Wang, S. Wang, *J. Hazard. Mater.* 291 (2015) 28.
- [42] M. Sheydaei, H.R. Karbor Shiadeh, B. Ayoubi-Feiz, R. Ezzati, *Chem. Eng. J.* 353 (2018) 138.
- [43] J. Xiao, Y. Xie, H. Cao, *Chemosphere* 121 (2015) 1.

- [45] H.H.A. Kosar, H. Miessner, S. Mueller, D. Kalass, D. Moeller, I. Khorshid, M.A.M. Rashid, *Chem. Eng. J.* 313 (2017) 1033.
- [46] A. Hassani, A. Khataee, S. Karaca, M. Fathinia, *J. Environ. Chem. Eng.* 5 (2017) 1964.
- [47] A. Alinejad, H. Akbari, M. Ghaderpoori, A. Khani Jeihooni, A. Adibzadeh, *Royal Society of Chemistry*, 9, 2019 8204.
- [48] O. Gimeno, J. Garcia-Araya, F. Beltran, F. Rivas, A. Espejo, *Chem. Eng. J.* 290 (2016) 12.
- [49] J. Yang, J. Xiao, H. Cao, Z. Guo, J. Rabeah, A. Brueckner, Y. Xie, *J. Hazard. Mater.* 360 (2018) 481.
- [50] P. Eskandari, M. Farhadian, A.R. Solaimany Nazar, *J. Chem. Technol. Biotechnol.* 92 (2017) 2360.
- [51] H. Bahrami, A. Eslami, R. Nabizadeh, A. Mohseni-Bandpi, A. Asadi, M. Sillanpää, *J. Clean. Prod.* 198 (2018) 1210.
- [53] A. Manafi, M. Hosseini, A. Fakhri, V.K. Gupta, S. Agarwal, *J. Mol. Liq.* 289 (2019), 110950.
- [54] A. Arimi, M. Farhadian, A.R. Solaimany Nazar, M. Homayoonfal, *Res. Chem. Intermed.* 42 (2016) 4021.
- [55] F. Zhou, H. Song, H. Wang, S. Komarneni, C. Yan, *Appl. Clay Sci.* 166 (2018) 9.
- [56] S. Xu, D. Feng, W. Shangguan, *J. Phys. Chem. C* 113 (2009) 2463.
- [57] N. Davari, M. Farhadian, A.R. Solaimany Nazar, *Environ. Technol.* (2019) 1.
- [58] T.J. Al-Musawi, H. Kamani, E. Bazrafshan, A.H. Panahi, M.F. Silva, G. Abi, *Catal. Lett.* 149 (2019) 1186.
- [59] M. Fazilati, A.H. Hassani, A. Torabian, (2018).
- [60] P. Bansal, A. Verma, K. Aggarwal, A. Singh, S. Gupta, *Can. J. Chem. Eng.* 94 (2016) 1269.
- [61] A. Seid-Mohammadi, G. Asgarai, Z. Ghorbanian, A. Dargahi, *Sep. Sci. Technol.* (2019) 1.
- [62] D.A.C. Coledam, M.M.S. Pupo, B.F. Silva, A.J. Silva, K.I. B.Eguiluz, G.R. Salazar-Banda, J.M. Aquino, Electrochemical mineralization of cephalexin using a conductive diamond anode: A mechanistic and toxicity investigation, *Chemosphere* 168 (2017) 638–647.